A Lateralized Brain Network for Visuospatial Attention

Supplementary Methods and Results

Michel Thiebaut de Schotten *[1,2,3†], Flavio Dell'Acqua [1,3,4†], Stephanie J Forkel [1], Andrew Simmons [3,4,5], Francesco Vergani [6], Declan G.M. Murphy [1] and Marco Catani [1,3]

[1]*Natbrainlab, Department of Forensic and Neurodevelopmental Sciences, Institute of Psychiatry, King's College London, London, UK*

[2]*INSERM–UPMC UMR S 975, G.H. Pitié–Salpêtrière, Paris, France*

[3]*Department of Neuroimaging, Institute of Psychiatry, King's College London, London, UK*

[4]*National Institute for Health Research Biomedical Research Centre for Mental Health, London, UK.*

[5]*MRC Centre for Neurodegeneration Research, King's College London, UK*

[6]*Department of Neurosurgery, Royal Victoria Infirmary, Newcastle upon Tyne, UK*

[†]*Contributed Equally to this work*

**Corresponding Author: Michel Thiebaut de Schotten, Natbrainlab, Department of Forensic and Neurodevelopmental Sciences, King's College, Institute of Psychiatry, 16 De Crespigny Park, SE5 8AF London UK. Email: michel.thiebaut@gmail.com*

Nature Neuroscience: doi:10.1038/nn.2905

A – SUPPLEMENTARY METHODS

1- Spherical Deconvolution (SD) tractography.

New developments in diffusion imaging tractography[1] offer a unique opportunity to visualize the organization of human brain pathways and to verify the existence of anatomical connections previously described only in the monkey[2-4]. Diffusion imaging is a modification of conventional magnetic resonance imaging sequences that permits the quantification of the diffusion characteristics of water molecules inside biological tissues[1]. Given that cerebral white matter contains axons, and that water molecules diffuse more freely along axons than across them[5], it is possible to obtain *in vivo* estimates of white matter fiber orientation by measuring the diffusivity of water molecules along different directions[6]. Tractography algorithms are used to reconstruct white matter tracts in three dimensions by sequentially piecing together discrete and shortly spaced estimates of fiber orientation to form continuous trajectories[2, 4]. Tractography has previously been used to dissect a large number of white matter connections in the human brain and these in vivo reconstructions are very close to the post-mortem findings derived from classical blunt dissections[7, 8]. However, the existence of a dorsal parieto-frontal system network similar to that described in the monkey[9, 10] has proven difficult to ascertain in the human brain[11]. This is due to the limitations of current tractography methods based on the diffusion tensor model, which provide only a single average estimate of the fiber orientation for each voxel. In voxels with crossing, kissing or fanning fibers, the tensor model is therefore unable to describe the complexity of the white matter organization and the resultant tractography reconstructions are likely to contain artefacts[4, 12]. Spherical Deconvolution (SD) tractography partially overcomes these limitations by modelling the diffusion signal as a distribution of multiple fiber orientations. Therefore with SD the number and orientations of different fiber populations can be identified and quantified within each voxel[13]. For further information on the SD method see[13].

Nature Neuroscience: doi:10.1038/nn.2905

2- Subjects

Twenty healthy right-handed volunteers (11 males and 9 females) aged between 22-38 years were recruited. All subjects gave written consent and were left-to-right readers. Handedness was estimated using the Edinburgh handedness test[14], which ranges from -100 for extremely left handed to +100 for extremely right-handed participant. A semi-structured interview was used to exclude those subjects with a previous history of neurological and psychiatric disorders. None of the participants were on medication. Demographic data and test results are reported in Supplementary Table 1.

Nature Neuroscience: doi:10.1038/nn.2905

Supplementary Table 1: Demographic data, performances and confidence intervals (CI 95%) of the participants

Participant	Age	Sex	Handedness	Bisection(mm)± CI 95%	Reaction time(index)± CI 95%	SLF I (index)	SLF II (index)	SLF III (index)
S01	37	M	+80	2.4 ± 1.68	0.0165 ± 0.0407	-0.0162	-0.0481	0.3968
S02	30	M	+100	-3.1 ± 1.61	-0.0353 ± 0.0411	0.3135	0.0908	0.3469
S03	27	M	+100	-4.0 ± 1.01	0.0075 ± 0.0358	0.1677	0.0406	0.5750
S04	23	F	+60	0.4 ±1.10	0.0430 ± 0.0297	0.2238	-0.1235	-0.0136
S05	32	M	+100	-1.0 ± 4.58	-0.0418 ± 0.0729	0.0737	0.0606	0.2597
S06	27	F	+100	-6.7 ± 1.94	-0.0638 ± 0.2042	-0.2032	0.1696	0.3998
S07	32	F	+100	0.2 ± 1.77	0.0129 ± 0.0733	-0.0778	-0.1604	0.2733
S08	28	F	+100	-0.4 ± 1.49	0.0167 ± 0.0893	-0.0241	0.2322	0.0903
S09	25	F	+100	-3.7 ± 1.01	-0.0327 ± 0.0402	-0.3189	0.2480	0.1784
S10	28	F	+100	-1.1 ± 1.12	-0.0246 ± 0.0459	-0.1421	0.1336	0.2328
S11	35	M	+100	-3.0 ± 2.28	-0.0110 ± 0.0377	-0.1127	0.2420	0.5540
S12	25	F	+100	-0.2 ± 1.17	0.0249 ± 0.0371	-0.2952	-0.0472	0.3699
S13	22	M	+100	1.6 ± 1.15	0.0302 ± 0.0241	0.2253	-0.2553	-0.1421
S14	26	M	+100	-1.2 ± 0.70	0.0158 ± 0.0680	0.0236	0.0516	0.1333
S15	32	M	+100	-1.7 ± 1.13	-0.0305 ± 0.1769	0.2169	0.0825	0.3101
S16	38	M	+100	-2.6 ± 2.09	-0.0562 ± 0.0823	-0.3732	0.1461	0.1568
S17	24	F	+100	-1.1 ± 1.07	-0.0081 ± 0.0923	-0.0029	-0.0824	0.5794
S18	25	M	+100	-2.7 ± 1.34	0.0157 ± 0.0701	-0.1670	0.1455	0.0346
S19	25	M	+100	0.8 ± 1.54	0.0216 ± 0.1956	0.3377	-0.3207	0.2552
S20	33	F	+100	-3.5 ± 0.98	0.0216 ± 0.0867	-0.0074	0.2477	0.2287

3- MRI data acquisition

For each participant, 60 contiguous near-axial slices were acquired on a 3T GE Signa HDx TwinSpeed system (General Electric, Milwaukee, WI, USA) with the following parameters: rostro-caudal phase encoding, voxel size 2.4x2.4x2.4 mm, matrix 128x128, slices 60, NEX 1, TE 93.4 ms, b-value 3000 s/mm^2, 60 diffusion-weighted directions and 7 non-diffusion-weighted volumes, using a spin-echo EPI sequence. Peripheral cardiac gating was applied with effective TR of 20/30 R-R intervals.

A sagittal three-dimensional MPRAGE data set covering the whole head was also acquired (166 slices, voxel resolution=1.2x1x1 mm, TE=2.8 ms, TR=7 ms, flip angle= 8°).

4- Diffusion MRI data processing

4.1- Correction for motion and eddy current distortion and estimation of the fiber orientation

Diffusion datasets were corrected for head motion and eddy current distortions using affine registration to a non diffusion-weighted reference volume[15] as implemented in the FSL software package[16].

White matter orientation estimation was performed using a spherical deconvolution (SD) approach[17, 18]. SD was chosen to estimate multiple orientations in voxels containing different populations of crossing fibres[19]. SD was applied using a modified (damped) version of the Richardson-Lucy algorithm[13]. The damped Richardson-Lucy algorithm reduces partial volume effects and spurious fiber orientations by providing reliable estimates of the fiber orientation distribution (FOD) in voxels, which include mixed contributions of white matter, grey matter and cerebro-spinal fluid. Algorithm parameters were chosen as described before[13]. Fiber orientation estimates were obtained selecting the orientation corresponding to the peaks (local maxima) of the FOD profiles. To exclude spurious local maxima we applied an absolute and a relative threshold. A first "absolute" threshold was used to exclude small local maxima due to noise or isotropic tissue. This

threshold is three times the amplitude of a spherical FOD obtained from a grey matter isotropic voxel. A second "relative" threshold of 5% of the maximum amplitude of the FOD was applied to remove the remaining local maxima with values greater than the absolute threshold[20].

4.2- Tractography algorithm

Whole brain tractography was performed selecting every brain voxel with at least one fiber orientation as a seed voxel. From these voxels and for each fiber orientation a modified fiber assignment by continuous tracking (FACT) algorithm[3] was used to reconstruct streamlines[21]. Streamlines were reconstructed by sequentially piecing together discrete and shortly spaced estimates of fiber orientation to form continuous trajectories. When entering a region with crossing white matter bundles the algorithm followed the orientation vector of least curvature[22]. Streamlines were halted when a voxel without fiber orientation was reached or when the curvature between two steps exceeded a threshold of 45°. The software estimating and reconstructing the orientation vectors and the trajectories from diffusion MRI was written in Matlab 7.8 (http://www.matwork.com). Full brain tractography of three representative subjects are displayed using TrackVis[23] (http://www.trackvis.org) as shown in Supplementary Figure 1.

Nature Neuroscience: doi:10.1038/nn.2905

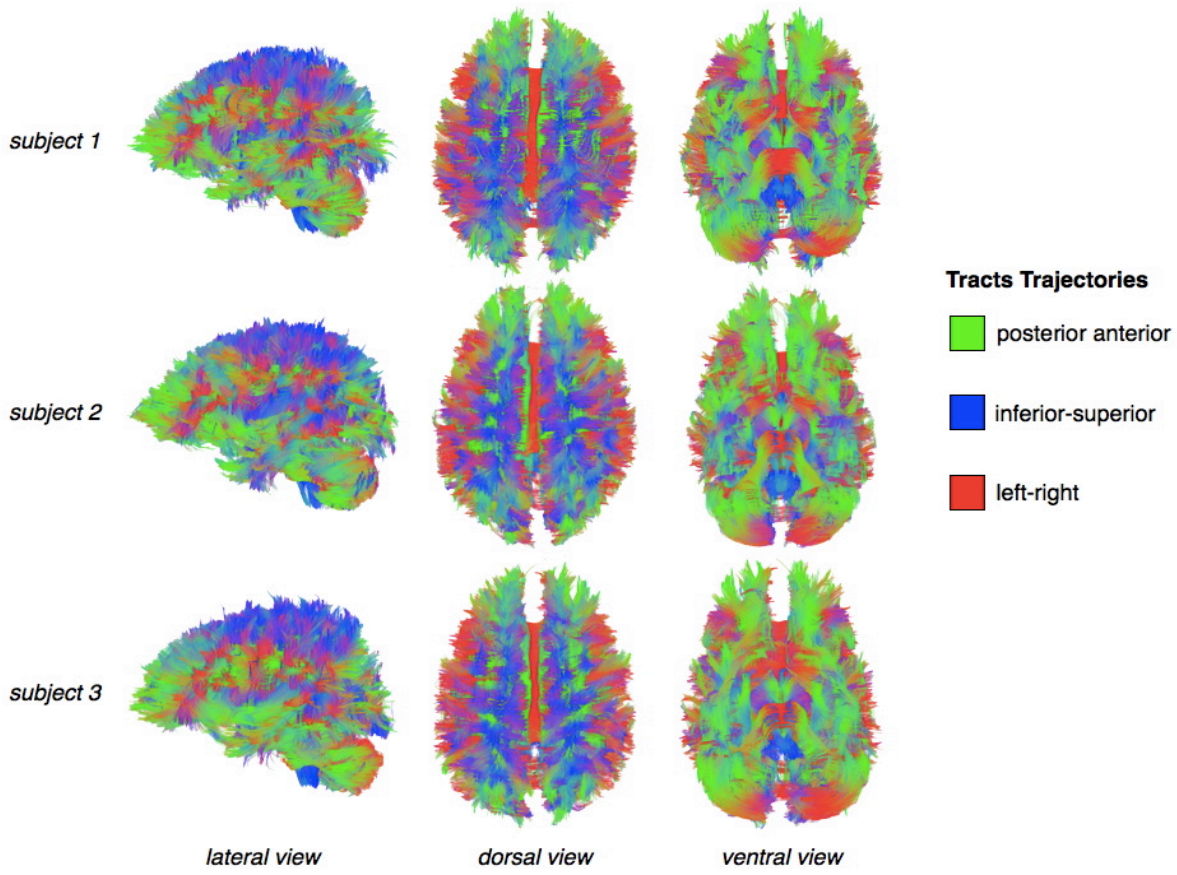

Supplementary Figure 1: Whole brain SD tractography using modified FACT algorithm of three representative subjects.

Nature Neuroscience: doi:10.1038/nn.2905

5- Parieto-frontal connections. Tractography dissections

5.1- Segmentation of the subcomponents of the parietal-frontal pathways

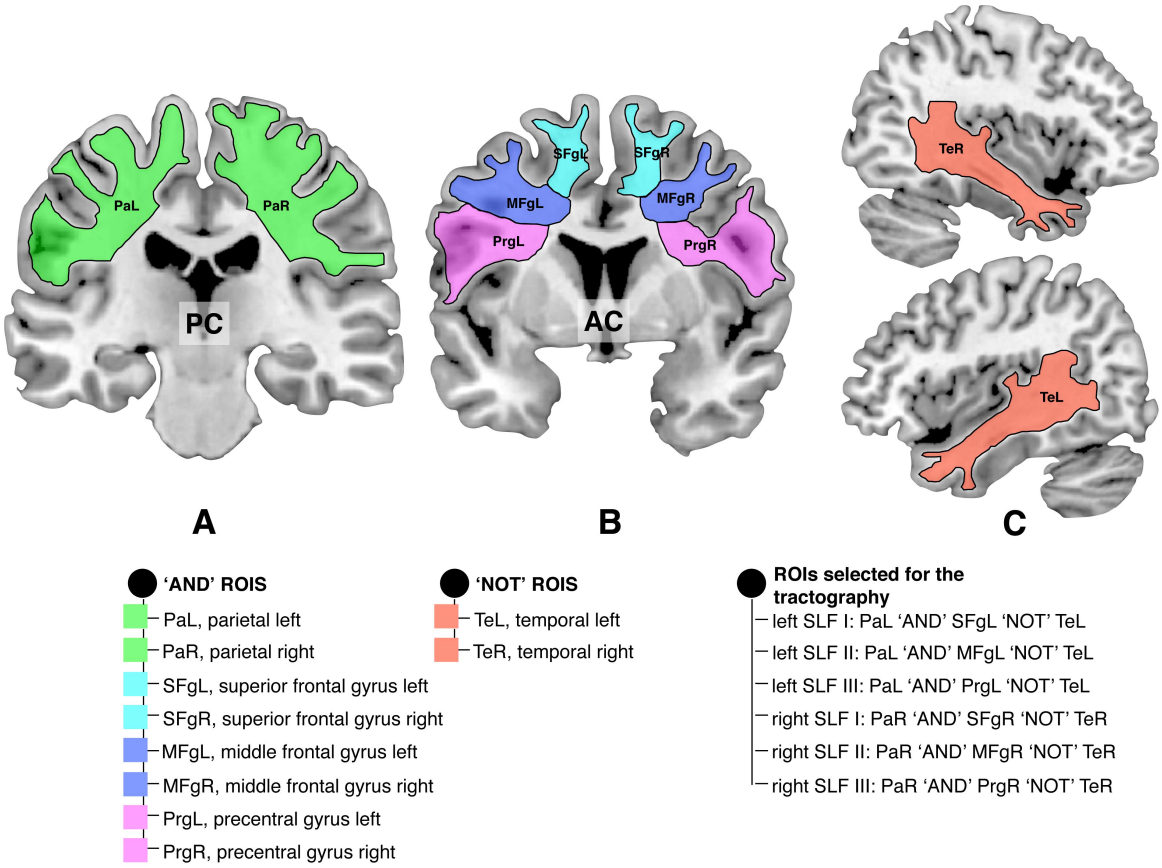

Supplementary Figure 2: Delineation of the regions of interest (ROI) used for the tractography of the three subcomponents of the left and right parieto-frontal connections. (A) Parietal ROIs in the left (PaL) and right (PaR) hemispheres. (B) Frontal ROIs in the left (SFgL, MFgL and PrgL) and right (SFgR, MFgR and PrgR) hemispheres. (C) Temporal ROI used to exclude the connections belonging to the temporo-frontal arcuate fasciculus in the left (TeL) and the right (TeR) hemispheres.

A multiple region of interests (ROIs) approach was used to isolate different components of the parieto-frontal network. Three ROIs were delineated around the white matter of the superior, middle and inferior/precentral frontal gyri, and another three 'AND' ROIs were delineated posteriorly in the parietal region. Streamlines of the arcuate

Nature Neuroscience: doi:10.1038/nn.2905

fasciculus projecting to the temporal lobe were excluded using a 'NOT' ROI in the temporal white matter (the arcuate is not part of the parieto-frontal system as it projects to the temporal lobe) (Supplementary Figure 2). Results from the three representative subjects are shown in Supplementary Figure 3. There was no significant difference between the number of voxels in the left and right superior frontal gyri ROIs (SFg; $t_{(19)} = -1.306$; $p = 0.207$), middle frontal gyri ROIs (MFg; $t_{(19)} = -0.036$; $p = 0.972$), precentral gyri ROIs (Prg; $t_{(19)} = -0.821$; $p = 0.422$), parietal ROIs (Pa; $t_{(19)} = -0.343$; $p = 0.735$) and temporal ROIs (Te; $t_{(19)} = 1.274$; $p = 0.218$).

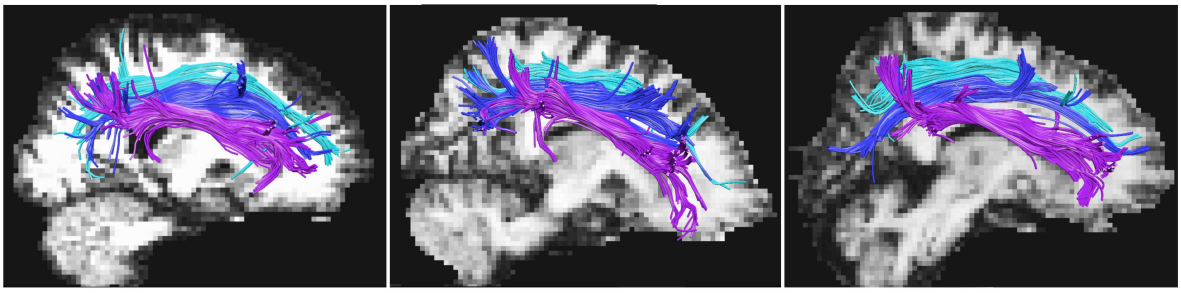

Supplementary Figure 3: Tractography reconstruction of the three branches of the parieto-frontal connections in three subjects. The most dorsal component (shown in light blue), the middle component (shown in navy blue) and the ventral component (shown in purple) correspond to the first, second and third branch of the superior longitudinal fasciculus (SLF I, II and III) respectively described in the monkey brain[9, 10].

5.2- Post-mortem validation of the SLF I, II and III.

Human post-mortem Klingler dissections[24] of the three SLF branches were performed on the right hemisphere, obtained from the autopsy of a 80 year-old woman's brain. This hemisphere was fixed in formalin for at least one year and then frozen at -15°C for two weeks. As described in Martino et al.[25] the water crystallization induced by the frozen process disrupts the structure of the gray matter and spreads the white matter fibers, facilitating the dissection of the fiber tracts. The SLF III and SLF II were exposed using

Nature Neuroscience: doi:10.1038/nn.2905

lateral surface to medial surface dissections. The SLF I was exposed using medial surface to lateral surface dissections (Supplementary figure 4).

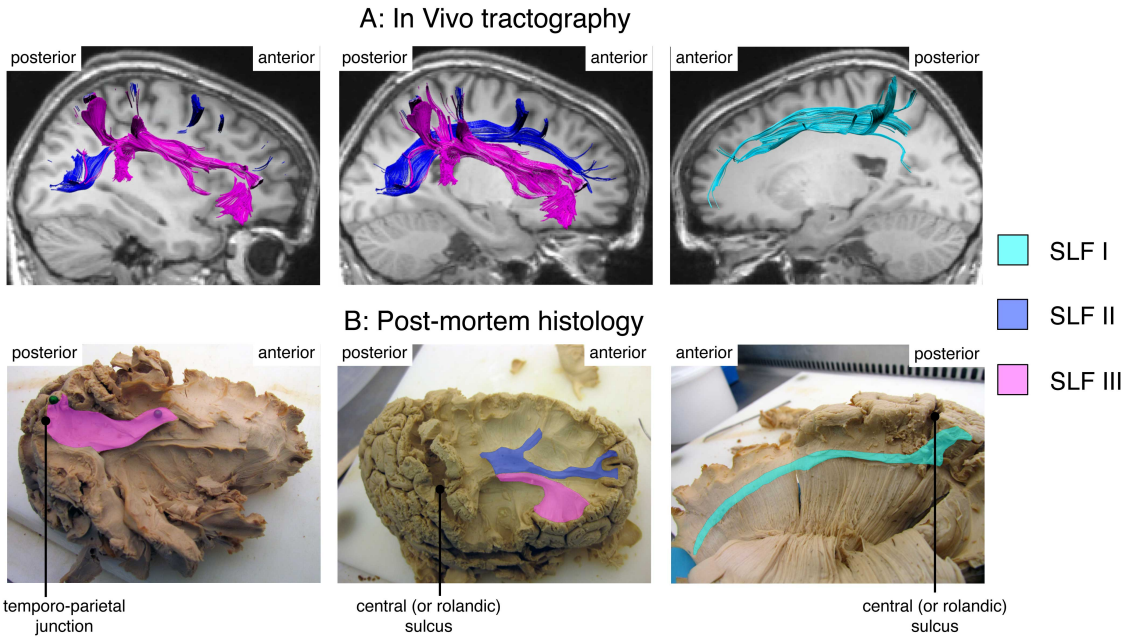

Supplementary Figure 4: Side-by-side comparison of the SLF I (in light blue), II (in navy blue) and III (in purple) obtained after a virtual dissection of a human living brain (A) and a real dissection of a post-mortem brain (B).

6- Atlasing the three branches of the SLF in the stereotaxic space.

6.1- Mapping of the pathway.

For each component of the parietal-frontal network binary visitation maps were created by assigning each voxel a value of 1 or 0 depending on whether the voxel was intersected by the streamlines of the tract[26-28]. These maps were normalized to the Montreal Neurological Institute (MNI) stereotaxic atlas and smoothed (full width half maximum=4*4*4) using SPM (http://www.fil.ion.ucl.ac.uk/spm). The smoothed and normalized visitation maps were then entered into a design matrix for a one-sample t-test corrected for Family Wise Error (FWE). Full details of this approach are given in[29]. Coronal sections of the result are shown in main Figure 2.

Nature Neuroscience: doi:10.1038/nn.2905

6.2- Cortical projections

To visualize the cortical projections of the three components of the parieto-frontal networks Trackvis software was used to extract the endpoint of each streamline. Binary visitation maps of the tractography endpoints for each subcomponent of the SLF were normalized to MNI space and smoothed using the same approach described above. The smoothed and normalized tractography endpoints maps were then entered into a design matrix for a one-sample t-test corrected for Family Wise Error (FWE). Results were projected onto the average 3D rendering of the internal cortical layer of the 20 participants in figure 1C. A similar approach has been reported in[30]. Supplementary Table 2 reports the T values and the coordinates of the local maxima of each cluster revealed by the group effect analysis.

Supplementary table 2: T value and MNI coordinates at the local maxima of each significant cluster of the SLF I, II and III

Parieto-frontal Subcomponent	Cluster volume (mm3)	Coordinates (mm,)			T value	*p* value(cluster) FWE corrected
		x	y	z		
SLF I Left	15538	-9	-45	53	8.34	0.001
	12724	-15	26	32	5.54	0.001
SLF I Right	14324	5	-43	52	5.15	0.001
	11826	17	22	42	5.27	0.001
SLF II Left	2980	-27	-44	30	5.15	0.014
	2916	-31	6	48	5.54	0.015
SLF II Right	7591	38	-59	23	5.11	0.001
	6181	32	14	40	4.47	0.001
SLF III Left	6314	-45	-42	31	7.52	0.001
	4426	-44	10	13	4.83	0.001
SLF III Right	10167	47	-36	35	18.80	0.001
	20671	41	13	15	7.72	0.001

7- Behavioral measures

Nature Neuroscience: doi:10.1038/nn.2905

7.1- Line bisection

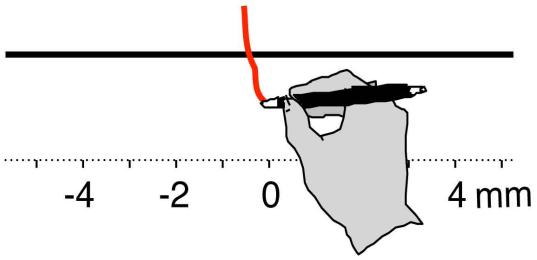

Supplementary Figure 5: Diagram of the line bissection

The line bisection paradigm consisted of twenty cm long, 1-mm thick black lines centered on a horizontal A4 sheet (one line per sheet) presented aligned to the subjects' eye-axis, in a central position relative to the patient's sagittal head plane. Subjects were instructed to mark the center of each line with a pencil. Each subject marked 10 lines in total, 5 with the left hand and 5 with the right hand. The deviation from the true centre was recorded and an average of the performance with both hands was used to perform correlation analysis with the tractography lateralization indexes.

7.2- Posner paradigm

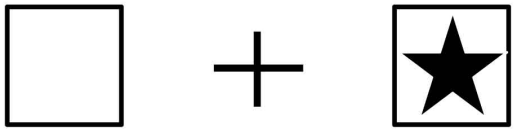

Supplementary Figure 6: Diagram of the modified Posner paradigm

The reaction time task consisted of a modification of the Posner paradigm[31]. The display contained a central fixation point and two boxes (unfilled squares) one on each side of the screen. The participants were asked to fixate on the central point and were instructed to press a button with the right hand each time they saw a star appearing in one of the two boxes. The reaction time (RT) was recorded in milliseconds. Before the appearance of the star, an arrow was briefly presented that pointed either to the left or right. The whole session consisted of 50% of trials with a valid cue (arrow pointing in the direction of the

Nature Neuroscience: doi:10.1038/nn.2905

star) and 50% of trials with an invalid cue (arrow pointing in the opposite direction of the star). The inter-trial interval was randomized between 4760-9440 ms.

8- Statistical analysis.

Statistical Analysis. Statistical analysis was performed using SPSS software (SPSS, Chicago, IL). A lateralization index was calculated for the volume of the three branches of the SLF according to the following formula:

Lateralisation index = (Right volume – Left volume)/(Right volume + Left volume).

Negative values indicate a leftward volume asymmetry and positive values a rightward asymmetry. A lateralization index of the detection time was calculated in a similar manner to that calculated for the volume of the SLF.

In our analysis, Gaussian distribution was confirmed for all the dependant variables using the Shapiro–Wilk test. This allows the use of standard parametric statistics in our dataset to draw statistical inferences. A one-sample t test (test value = 0) was used to assess the lateralization of the volume in voxels of the SLF I, II and III. Pearson correlation analysis was performed between the lateralization index of the three branches of the superior longitudinal fasciculus (volume in voxels) and the behavioral performances. We identified 1 outlier for the line bisection (more than two standard deviation from the mean) that we removed from the correlation analyses.

Nature Neuroscience: doi:10.1038/nn.2905

B – SUPPLEMENTARY RESULTS

1- Rhesus Monkey SLF I, II and III

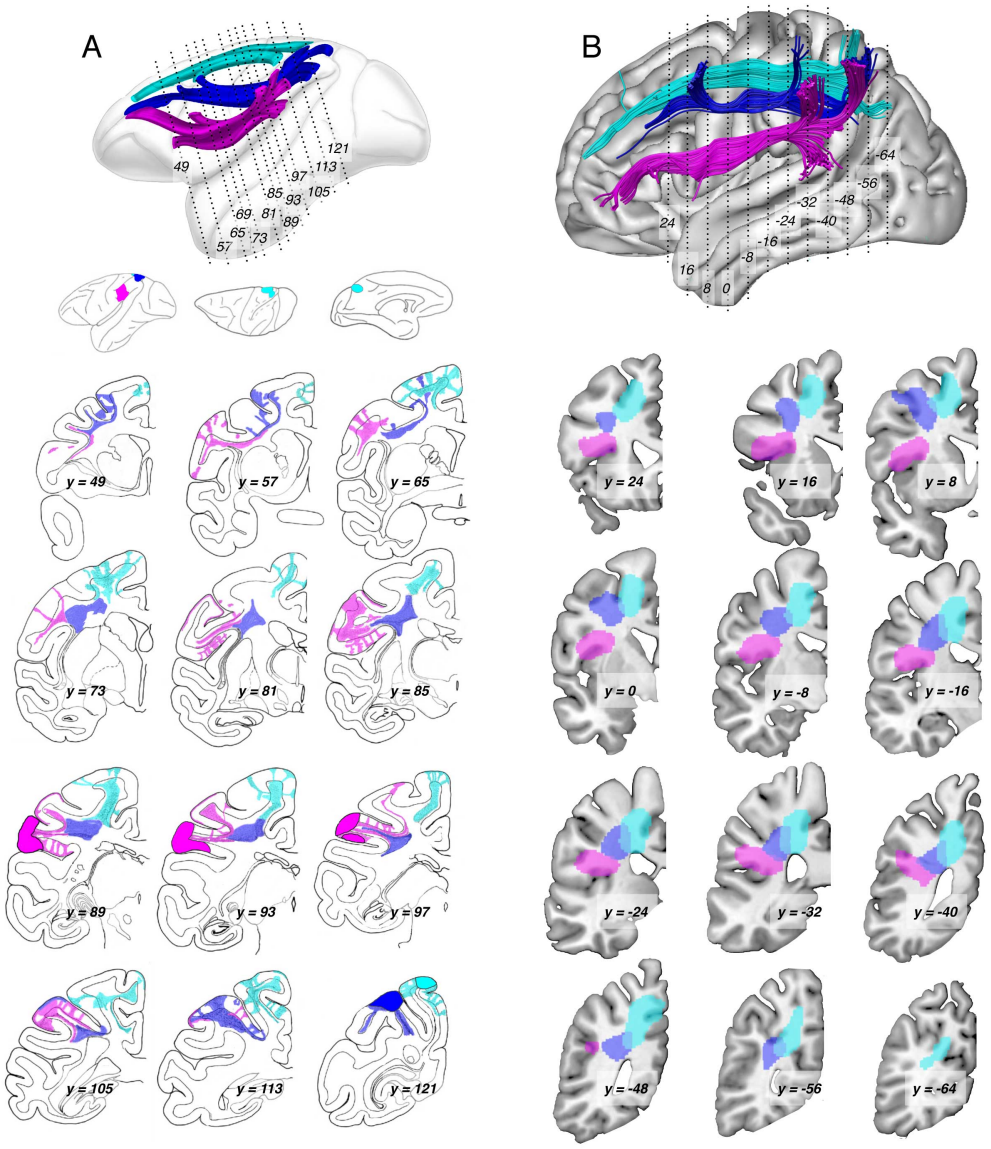

Supplementary Figure 7: Reconstruction of the three branches of the SLF: comparison between post-mortem axonal tracing in monkey (A)[9, 10] and in vivo SD tractography in humans (B).

Nature Neuroscience: doi:10.1038/nn.2905

The monkey maps of the SLF I, II and III presented in supplementary Figure 7 are modified from the coronal slices provided in an Atlas by Schmahmann & Pandya[10]. The modification consists of coloring the tract in light blue (SLF I), navy blue (SLF II) and purple (SLF III) according to the site of injection for the axonal tracing. Projection and commissural fibers have been removed for the purpose of visualization.

Supplementary Figure 7 shows side by side the virtual in vivo dissections from our study and corresponding slices from a monkey atlas[10] that we have modified for direct comparison. Overall parieto-frontal connections of the human and the monkey brain are organized similarly in three longitudinal pathways. In humans, the most dorsal pathway originates from the precuneus and the superior parietal lobule (Brodmann areas, BA 5 and 7); and projects to the superior frontal and anterior cingulate gyri (BA 8, 9 and 32). This pathway corresponds to the first branch of the superior longitudinal fasciculus (SLF I) as described in the monkey brain[9, 10, 22]. In contrast the middle pathway originates in the anterior intermediate parietal sulcus and the angular gyrus (BA 39 and 40) and ends in the posterior regions of the superior and middle frontal gyri (BA 8 and 9). This pathway corresponds to the SLF II in the monkey brain[9, 10, 22]. Lastly, the most ventral pathway originates in the temporo-parietal junction (BA 40) and terminates in the inferior frontal gyrus (BA 44, 45 and 47); corresponding to the SLF III in the monkey brain[9, 10, 22]. We were also able to replicate our in vivo findings using post-mortem blunt dissections in a human brain (see supplementary Figure 4). Although the post-mortem dissections were limited in identifying the exact cortical projections of the three SLF, a good correspondence was found between post-mortem and in vivo dissections of the central course of the three branches. Overall our results suggest a strong similarity between monkey and human parieto-frontal connections.

2- Functional activation studies

Nature Neuroscience: doi:10.1038/nn.2905

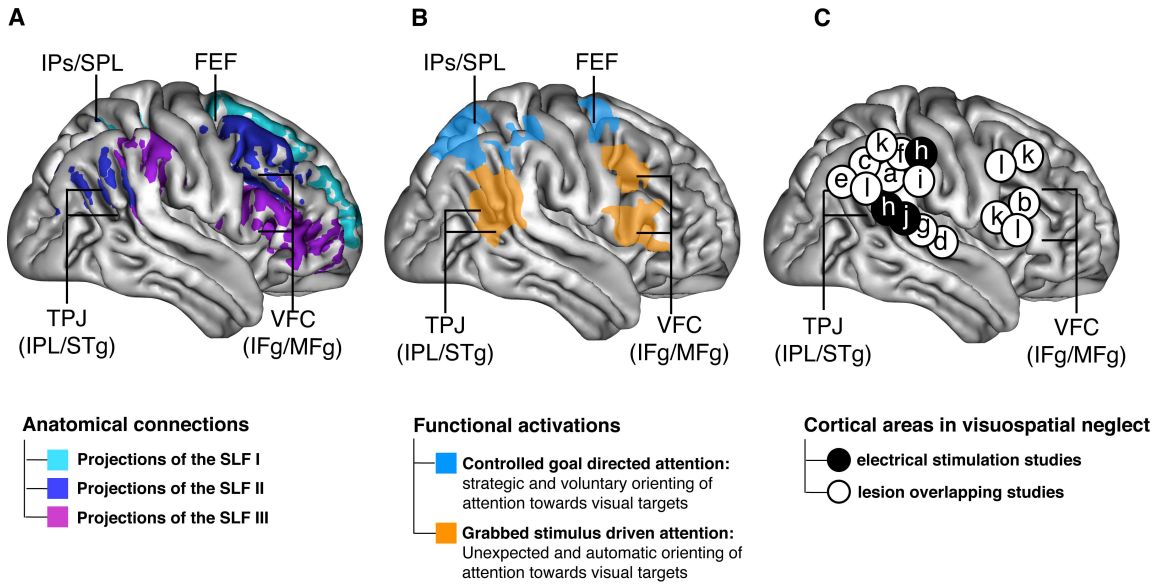

Supplementary Figure 8: The parieto-frontal networks for visuo-spatial attention as identified by tractography (A), functional neuroimaging (B) and brain lesion/electrical stimulation (C) studies. The SLF I projects to areas activated in tasks requiring controlled goal directed attention, whereas the SLF III projects towards areas activated during tasks requiring automatic reorienting of spatial attention to unexpected stimuli. The cortical projections of the SLF II overlap with both dorsal and ventral functional networks (B adapted from[32]). Disorders of spatial attention are frequently associated with either cortical or subcortical lesions of the ventral parieto-frontal network (C) a[33], b[34], c[35], d[36], e[37], f[38], g[39], h[40], i[41], j[42], k[43], l[44] IPs: intraparietal sulcus; SPL: superior parietal lobule, FEF: frontal eye field, TPJ: temporo-parietal junction, IPL: inferior parietal lobule, STg: superior temporal gyrus, VCF: ventral frontal cortex, IFg: inferior frontal gyrus, MFg: middle frontal gyrus.

The figure summarizing the functional activation studies (fMRI and PET) presented in supplementary figure 8 was adapted from the work of Corbetta et al.[32]. In particular the studies involved tasks for the detection of cortical functional activation during two conditions: i) strategic and voluntary orienting of spatial attention towards visual targets[45-48]; ii) unexpected and automatic orienting of attention towards visual targets[49-54]. Foci of activation reported in Corbetta et al.[32], were projected onto the average 3D rendering of the internal cortical layer of the 20 participants used in our study.

Nature Neuroscience: doi:10.1038/nn.2905

3- Brain lesion studies

The summary figure of the brain lesion and electrical stimulation studies presented in Figure 2 was created using all the studies previously published in the literature. A comprehensive search of group studies with PUBMED identified 10 brain lesion studies a[33], b[34], c[35], d[36], e[37], f[38], g[39], i[41], k[43], l[44] and 2 intraoperative electrical stimulation studies h[40] and j[42]. Foci of maximum overlap of the lesion or electrical stimulation were projected onto the average 3D rendering of the internal cortical layer of the 20 participants.

Nature Neuroscience: doi:10.1038/nn.2905

C – SUPPLEMENTARY NOTE

Although the SLF III shows the most significant rightward lateralization, this did not correlate with the line bisection performance and the speed of visuospatial processing. A possible explanation may be that the SLF III has a key role in sustained attention and novelty processing, which have not been measured in our study[32, 55, 56]. Furthermore the function of the SLF III differs between the two hemispheres. In the left hemisphere the SLF III projects to areas involved in verbal fluency[57] and praxis[58]. In the right hemisphere the SLF III projects to areas involved in visuospatial attention[32], prosody[59] and music processing[60]. Hence, this suggests that an anatomical asymmetry of the brain should not be taken as direct evidence of hemispheric dominance as the correlation between anatomical lateralization and specialization of functions is not straightforward.

Further, in this study the number of voxels visited by the reconstructed streamlines was used as a surrogate measure of the tract volume. It is, however, important to highlight that the number of visited voxels does not represent the true tract volume but rather quantifies the space occupied by the reconstructed tract. Hence, factors such as multiple fiber crossing, fanning or kissing[4] can affect the ability to reconstruct streamlines and therefore the overall volume estimate. In this study we used SD tractography to minimize this bias by tracking through regions with multiple fiber orientations. It is however still possible that smaller branches of the SLF were not reconstructed due to the relatively large voxels size resolution of our datasets.

Nature Neuroscience: doi:10.1038/nn.2905

11- Supplementary references

1. Le Bihan, D. & Breton, E. Imagerie de diffusion in-vivo par résonance magnétique nucléaire. *Comptes rendus de l'Académie des sciences* **301**, 1109-1112 (1985).
2. Jones, D.K., Simmons, A., Williams, S.C. & Horsfield, M.A. Non-invasive assessment of axonal fiber connectivity in the human brain via diffusion tensor MRI. *Magn Reson Med* **42**, 37-41 (1999).
3. Mori, S., Crain, B.J., Chacko, V.P. & van Zijl, P.C. Three-dimensional tracking of axonal projections in the brain by magnetic resonance imaging. *Ann Neurol* **45**, 265-269 (1999).
4. Basser, P.J., Pajevic, S., Pierpaoli, C., Duda, J. & Aldroubi, A. In vivo fiber tractography using DT-MRI data. *Magn Reson Med* **44**, 625-632 (2000).
5. Moseley, M.E*., et al.* Diffusion-weighted MR imaging of anisotropic water diffusion in cat central nervous system. *Radiology* **176**, 439-445 (1990).
6. Basser, P.J., Mattiello, J. & Le Bihan, D. MR diffusion tensor spectroscopy and imaging. *Biophys J* **66**, 259-267 (1994).
7. Catani, M., Howard, R.J., Pajevic, S. & Jones, D.K. Virtual in vivo interactive dissection of white matter fasciculi in the human brain. *NeuroImage* **17**, 77-94 (2002).
8. Catani, M. & Thiebaut de Schotten, M. A diffusion tensor imaging tractography atlas for virtual in vivo dissections. *Cortex* **44**, 1105-1132 (2008).
9. Petrides, M. & Pandya, D.N. Projections to the frontal cortex from the posterior parietal region in the rhesus monkey. *J. Comp. Neurol.* **228**, 105-116 (1984).
10. Schmahmann, J.D. & Pandya, D.N. *Fiber Pathways of the Brain* (Oxford University Press, Oxford, 2006).
11. Makris, N*., et al.* Segmentation of subcomponents within the superior longitudinal fascicle in humans: a quantitative, in vivo, DT-MRI study. *Cereb Cortex* **15**, 854-869 (2005).
12. Jones, D.K. Studying connections in the living human brain with diffusion MRI. *Cortex* **44**, 936-952 (2008).
13. Dell'acqua, F*., et al.* A modified damped Richardson-Lucy algorithm to reduce isotropic background effects in spherical deconvolution. *Neuroimage* **49**, 1446-1458 (2010).
14. Oldfield, R.C. The assessment and analysis of handedness: the Edinburgh inventory. *Neuropsychologia* **9**, 97-113 (1971).
15. Jenkinson, M. & Smith, S. A global optimisation method for robust affine registration of brain images. *Medical image analysis* **5**, 143-156 (2001).
16. Smith, S.M*., et al.* Advances in functional and structural MR image analysis and implementation as FSL. *Neuroimage* **23 Suppl 1**, S208-219 (2004).
17. Tournier, J.D., Calamante, F., Gadian, D.G. & Connelly, A. Direct estimation of the fiber orientation density function from diffusion-weighted MRI data using spherical deconvolution. *NeuroImage* **23**, 1176-1185 (2004).
18. Tournier, J.D., Calamante, F. & Connelly, A. Robust determination of the fibre orientation distribution in diffusion MRI: non-negativity constrained super-resolved spherical deconvolution. *Neuroimage* **35**, 1459-1472 (2007).

19. Alexander, D.C. An introduction to computational diffusion MRI: the diffusion tensor and beyond. in *Visualization and Processing of Tensor Fields* 83-106 (Springer, Berlin, 2006).
20. Dell'Acqua, F.*, et al.* Mapping Crossing Fibres of the Human Brain with Spherical Deconvolution: Towards an Atlas for Clinico-Anatomical Correlation Studies *Proc. Intl. Soc. Mag. Reson. Med.* **17**, 3562 (2009).
21. Descoteaux, M., Deriche, R., Knösche, T.R. & Anwander, A. Deterministic and probabilistic tractography based on complex fibre orientation distributions. *IEEE transactions on medical imaging* **28**, 269-286 (2009).
22. Schmahmann, J.D.*, et al.* Association fibre pathways of the brain: parallel observations from diffusion spectrum imaging and autoradiography. *Brain* **130**, 630-653 (2007).
23. Wedeen, V.J.*, et al.* Diffusion spectrum magnetic resonance imaging (DSI) tractography of crossing fibers. *NeuroImage* **41**, 1267-1277 (2008).
24. Klingler, J. Erleichterung der makroskopischen Präparation des Gehirn durch den Gefrierprozess. *Schweiz Arch Neurol Psychiat* **36**, 247-256 (1935).
25. Martino, J., Brogna, C., Robles, S., Vergani, F. & Duffau, H. Anatomic dissection of the inferior fronto-occipital fasciculus revisited in the lights of brain stimulation data. *Cortex* (2009).
26. Catani, M.*, et al.* Symmetries in human brain language pathways correlate with verbal recall. *Proc Natl Acad Sci U S A* **104**, 17163-17168 (2007).
27. Lawes, I.N.C.*, et al.* Atlas-based segmentation of white matter tracts of the human brain using diffusion tensor tractography and comparison with classical dissection. *NeuroImage* **39**, 62-79 (2008).
28. Thiebaut de Schotten, M.*, et al.* Visualization of disconnection syndromes in humans. *Cortex* **44**, 1097-1103 (2008).
29. Thiebaut de Schotten, M.*, et al.* Atlasing location, asymmetry and inter-subject variability of white matter tracts in the human brain with MR diffusion tractography. *Neuroimage* **54**, 49-59 (2011).
30. Tsang, J.M., Dougherty, R.F., Deutsch, G.K., Wandell, B.A. & Ben-Shachar, M. Frontoparietal white matter diffusion properties predict mental arithmetic skills in children. *Proc Natl Acad Sci U S A* **106**, 22546-22551 (2009).
31. Posner, M.I. Orienting of attention. *Q J Exp Psychol* **32**, 3-25 (1980).
32. Corbetta, M. & Shulman, G.L. Control of goal-directed and stimulus-driven attention in the brain. *Nat Rev Neurosci* **3**, 201-215 (2002).
33. Vallar, G. & Perani, D. The anatomy of unilateral neglect after right-hemisphere stroke lesions. A clinical/CT-scan correlation study in man. *Neuropsychologia* **24**, 609-622 (1986).
34. Husain, M. & Kennard, C. Visual neglect associated with frontal lobe infarction. *J Neurol* **243**, 652-657 (1996).
35. Leibovitch, F.S.*, et al.* Brain-behavior correlations in hemispatial neglect using CT and SPECT: the Sunnybrook Stroke Study. *Neurology* **50**, 901-908 (1998).
36. Karnath, H.O., Ferber, S. & Himmelbach, M. Spatial awareness is a function of the temporal not the posterior parietal lobe. *Nature* **411**, 950-953 (2001).
37. Mort, D.J.*, et al.* The anatomy of visual neglect. *Brain* **126**, 1986-1997 (2003).

38. Doricchi, F. & Tomaiuolo, F. The anatomy of neglect without hemianopia: a key role for parietal-frontal disconnection? *Neuroreport* **14**, 2239-2243 (2003).
39. Karnath, H.O., Fruhmann Berger, M., Küker, W. & Rorden, C. The anatomy of spatial neglect based on voxelwise statistical analysis: a study of 140 patients. *Cereb Cortex* **14**, 1164-1172 (2004).
40. Thiebaut de Schotten, M.*, et al.* Direct evidence for a parietal-frontal pathway subserving spatial awareness in humans. *Science* **309**, 2226-2228 (2005).
41. Corbetta, M., Kincade, M., Lewis, C., Snyder, A. & Sapir, A. Neural basis and recovery of spatial attention deficits in spatial neglect. *Nat Neurosci* **8**, 1603-1610 (2005).
42. Gharabaghi, A., Fruhmann Berger, M., Tatagiba, M. & Karnath, H.O. The role of the right superior temporal gyrus in visual search-insights from intraoperative electrical stimulation. *Neuropsychologia* **44**, 2578-2581 (2006).
43. Committeri, G.*, et al.* Neural bases of personal and extrapersonal neglect in humans. *Brain* **130**, 431-441 (2007).
44. Verdon, V., Schwartz, S., Lovblad, K.O., Hauert, C.A. & Vuilleumier, P. Neuroanatomy of hemispatial neglect and its functional components: a study using voxel-based lesion-symptom mapping. *Brain* **133**, 880-894 (2010).
45. Corbetta, M., Kincade, J.M., Ollinger, J.M., McAvoy, M.P. & Shulman, G.L. Voluntary orienting is dissociated from target detection in human posterior parietal cortex. *Nat Neurosci* **3**, 292-297 (2000).
46. Hopfinger, J.B., Buonocore, M.H. & Mangun, G.R. The neural mechanisms of top-down attentional control. *Nat Neurosci* **3**, 284-291 (2000).
47. Kastner, S., Pinsk, M.A., De Weerd, P., Desimone, R. & Ungerleider, L.G. Increased activity in human visual cortex during directed attention in the absence of visual stimulation. *Neuron* **22**, 751-761 (1999).
48. Shulman, G.L.*, et al.* Areas involved in encoding and applying directional expectations to moving objects. *J Neurosci* **19**, 9480-9496 (1999).
49. Braver, T.S., Barch, D.M., Gray, J.R., Molfese, D.L. & Snyder, A. Anterior cingulate cortex and response conflict: effects of frequency, inhibition and errors. *Cereb Cortex* **11**, 825-836 (2001).
50. Clark, C.A. & Le Bihan, D. Water diffusion compartmentation and anisotropy at high b values in the human brain. *Magn Reson Med* **44**, 852-859 (2000).
51. Downar, J., Crawley, A.P., Mikulis, D.J. & Davis, K.D. A multimodal cortical network for the detection of changes in the sensory environment. *Nat Neurosci* **3**, 277-283 (2000).
52. Downar, J., Crawley, A.P., Mikulis, D.J. & Davis, K.D. The effect of task relevance on the cortical response to changes in visual and auditory stimuli: an event-related fMRI study. *Neuroimage* **14**, 1256-1267 (2001).
53. Kiehl, K.A., Laurens, K.R., Duty, T.L., Forster, B.B. & Liddle, P.F. Neural sources involved in auditory target detection and novelty processing: an event-related fMRI study. *Psychophysiology* **38**, 133-142 (2001).
54. Marois, R., Leung, H.C. & Gore, J.C. A stimulus-driven approach to object identity and location processing in the human brain. *Neuron* **25**, 717-728 (2000).
55. Wilkins, A.J., Shallice, T. & McCarthy, R. Frontal lesions and sustained attention. *Neuropsychologia* **25**, 359-365 (1987).

Nature Neuroscience: doi:10.1038/nn.2905

56. Singh-Curry, V. & Husain, M. The functional role of the inferior parietal lobe in the dorsal and ventral stream dichotomy. *Neuropsychologia* **47**, 1434-1448 (2009).
57. Schiff, H.B., Alexander, M.P., Naeser, M.A. & Galaburda, A.M. Aphemia. Clinical-anatomic correlations. *Arch Neurol* **40**, 720-727 (1983).
58. Heilman, K.M. & Watson, R.T. The disconnection apraxias. *Cortex* **44**, 975-982 (2008).
59. Ross, E.D. The aprosodias. Functional-anatomic organization of the affective components of language in the right hemisphere. *Arch Neurol* **38**, 561-569 (1981).
60. Loui, P., Alsop, D. & Schlaug, G. Tone deafness: a new disconnection syndrome? *J Neurosci* **29**, 10215-10220 (2009).

Nature Neuroscience: doi:10.1038/nn.2905